DOI: 10.13009/EUCASS2023-960
Aerospace Europe Conference 2023 – 10TH EUCASS – 9TH CEAS

Characterisation of tantalum and lanthanum hexaboride low-current heaterless hollow cathodes

Mathew Denys[⋆], *Jakub Glowacki*[⋆†], *Emile Webster*[⋆], *Cameron Shellard*[⋆], *Gennady Sidorov*[⋆],
Andrew Limmer-Wood[⋆⋆] *and Randy Pollock*[⋆]
[⋆]*Robinson Research Institute, Victoria University of Wellington, New Zealand*
[⋆⋆] *Canterbury University, Christchurch, New Zealand*
jakub.glowacki@vuw.ac.nz
[†]Corresponding author

Abstract

Hollow cathodes are widely utilised for plasma generation in electric thrusters. However, despite years of extensive development, cathode design and operation, especially the heaterless configuration remains an engineering challenge. This work presents a method of reaching a stable discharge mode and mitigation of operational instabilities. The analysis is presented through the comparative studies between cathodes of the two most commonly used emitters: open-end tantalum and embedded lanthanum hexaboride (LaB_6), operating with argon propellant. Arcing during the discharge is overcome using a current limiting circuit. The analysis concentrates on the transient regime between 0.2-1.4 A discharge and 0.5 - 6 mg/s propellant flow rate and identifies the minimum discharge power needed for reaching the thermionic emission. The electrical characterisation is used to guide thermal design analysis. The thermal model shows good agreement with measurements and proves to be a useful tool for predicting overall emission and temperature distributions in the cathode assembly. It is suspected that although the temperature of both emitters stays below 1400 K, it takes the LaB_6 emitter considerably longer (200s) to reach the same state as the tantalum. Additionally, the LaB_6 design is less prone to operational wear down, which became a problem after 10's of hours of operation using the open-ended tantalum cathode.

1. Introduction

Electric propulsion (EP) with its inherently high specific impulse is foreseen as an enabling technology for a large variety of space missions including station-keeping, orbital manoeuvring and deep space exploration. In recent years, due to the increase in the number of newly designed satellites, EP technology is gaining momentum.[1] Many decades of development have resulted in several thruster types, such as Hall Effect Thruster and Gridded Ion Thrusters which have now matured and proved their reliable operation on several space missions[2].[3] The progress fostered the development of sub-components including cathodes and hollow cathodes which serve as electron sources for electric thrusters and are critical for plasma ignition and plume neutralisation. Due to the years of development the basic operational principles have now been largely understood and well documented.[1] However, the excessive wear-down of cathode components and nuances related to instability effects, i.e. plasma oscillations, remains unresolved. Additionally, the application of recent findings to engineering practice is still challenging. These particularly manifest themselves in applications characterised by elevated design requirements[4].[5]

Research on cathodes has been mostly concentrated on heated cathodes which in their design embrace resistive heaters to warm up the emitter to a thermionic emission state.[6] This mode of operation adds additional complexity to the power processing unit and decreases the system's reliability. Heaterless hollow cathodes (HHC) are an alternative solution which relies on the discharge current to warm up the emitter to the emission state. They are characterised by design simplicity, and the ability to ignite the thruster almost instantly. Despite all of its advantages, the technology has several reported drawbacks mostly related to elevated voltage, mass flow rate requirements and occasional arcing[7] which consequently leads to rapid wear down.

The HHC development process plays a fundamental role in electric thruster design. Power and mass flow requirements to keep stable discharge are not only driving the size of the power processing unit but also impacting the thruster's thermal management. The latter aspect is particularly important due to the high temperature needed for reaching thermionic emission (>1500 K). This brings a challenge of cathode separation from the rest of thruster components to avoid overheating and becomes an important issue for systems with intrinsically restricted power and heat budgets, such as low-power thrusters[8] and new disruptive propulsion technologies,[9].[10]

DOI: 10.13009/EUCASS2023-960

This paper presents the development of HHC from the perspective of its application to power a kW-class magnetoplasmadynamic thruster (MPDT). This type of electric propulsion is characterised by a wide operational profile, can work with various propellants and is considered to be a high thrust-density solution. However, the high discharge current requirement has constrained its applicability. One of the development paths to widespread MPDTs is through the application of thermionic hollow cathodes. Previous work showed that the HHCs can develop conditions favourable to sustain discharges in the 1-5 kW range.[11] Such power demands can be met by current space platforms. MPDTs, however, still suffer from low efficiency[12] and different methods are being proposed to address the issue. The role of high magnetic fields is one of the active areas of research, and the application of superconducting magnets,[13][14] is envisioned as a possible path towards improving the efficiency of MPDTs. This however leads to additional strain on thermal control systems, where heat must be carefully managed between components in order to prevent failure of the cryogenic system.[15] From this perspective, it is of interest to reevaluate the role of cathode ignition, operation and thermal management to identify limits of stable operation on different types of HHCs while minimising heat dissipation to the system. This task is accomplished by a combination of experimental and numerical work, providing additional insight into the applicability of robust engineering tools based on Finite Element Methods to predict temperature distribution on electric thrusters. The proposed method discusses the validity of a combined experimental and numerical approach to solving engineering problems related to HHC.

2. Hollow Cathode characterisation

A schematic of the MPD thruster under development is presented in Figure 1a. An argon propellant line feeds into the rear of the HHC, which is centered inside a keeper anode. The HHC insert and keeper are electrically isolated; the insert is attached to the negative output of a DC power supply unit through the propellant line and the keeper is attached to the positive through the retainer body. The keeper is manufactured from stainless steel, with a removable threaded cap holding an orificed tantalum plate in place. The keeper orifice is subjected to extensive erosion so the design allows the tantalum plate to be exchanged. This also provides a mechanism to change the keeper orifice diameter during development. The cap is manufactured from titanium to prevent it from welding to the keeper's body during operation. A copper anode surrounds the insert–keeper assembly but is not directly relevant to the development and characterisation of the cathode under discussion in this paper. The entire assembly is mounted inside a 3 m^3 vacuum chamber with an initial vacuum pressure of $\sim 5 \times 10^{-6}$ mBar. During typical operation with a flow rate of 4 mg/s of Argon, the pressure rises to 2×10^{-4} mBar. The propellant flow is controlled by Alicat MC 500 mass flow controller outside the vacuum chamber. The thermal characterisation was verified by comparison with the temperature measurements at the propellant line using an N-type thermocouple. The thermocouple was a mineral-insulated metal sheath 1.5 mm in diameter with a 40 mm of contact distance. Approximated point of measurement was on the thermocouple bend 40 mm behind the retained (as shown in Fig.1a)

Two HHC designs are considered in this paper; the first utilises an emitter produced from a roll of tantalum (Figure 1b), while the other utilises a lanthanum hexaboride (LaB_6) emitter (Figure 1c). Both materials are desirable due to their low work functions ϕ , which allows full ignition at lower temperatures. As a result of high temperature, they reach a thermionic emission state emitting electrons to the propellant. The emission is described Richardson-Dushman equation, where current density j_e can be expressed as a function of temperature

$$j_e = A_0 T^2 e^{-e\phi/kT}, \tag{1}$$

where $A_0 = 1.20173 \times 10^6$ A $m^{-2}K^{-2}$ is a constant, e is electron charge, k Boltzmann constant and T is the temperature. LaB_6 emitters are characterised by work function of $\phi_{LaB_6} = 2.91$ eV,[16][17] and tantalum $\phi_{Ta} = 4.25$ eV.[18] As a result, the cathode based on LaB_6 emitter can reach thermionic emission at a temperature of 500 K lower than tantalum and can operate in the 1400-2000 K range. Thus, they are interesting from the perspective of low-current discharge applications.

The HHC ignition process involves first applying a large cathode–keeper voltage to induce a Paschen breakdown in the inert propellant. The resulting plasma heats the cathode's emitter to the point that the thermal energy of electrons overcomes its work function. Once in this mode of operation – "thermionic emission" – a plasma can be maintained with a reduced keeper voltage. A key issue to address is that when the plasma breakdown occurs it can result in either electric arcing, or a glow discharge. If the power supply is connected directly to the cathode and keeper, the breakdown tends to result in electric arcing.[7] Not only are these arcing events damaging to the cathode, but they exhaust the power supply's output capacitors on the order of 0.5 ms, preventing the formation of a stable plasma that can sufficiently heat the emitter to thermionic emission. As shown in the circuit diagram in Figure 2, the arcing was overcome by an adding resistive load, R_k, in series with the power supply and the keeper. Also in series with R_k is a sub-circuit involving an N-channel depletion mode MOSFET, providing a hard current limit in addition to R_k: as the current increases, R_{GS} causes the gate-source voltage to increase, turning the transistor "off". By adjusting the value of R_{GS}

DOI: 10.13009/EUCASS2023-960

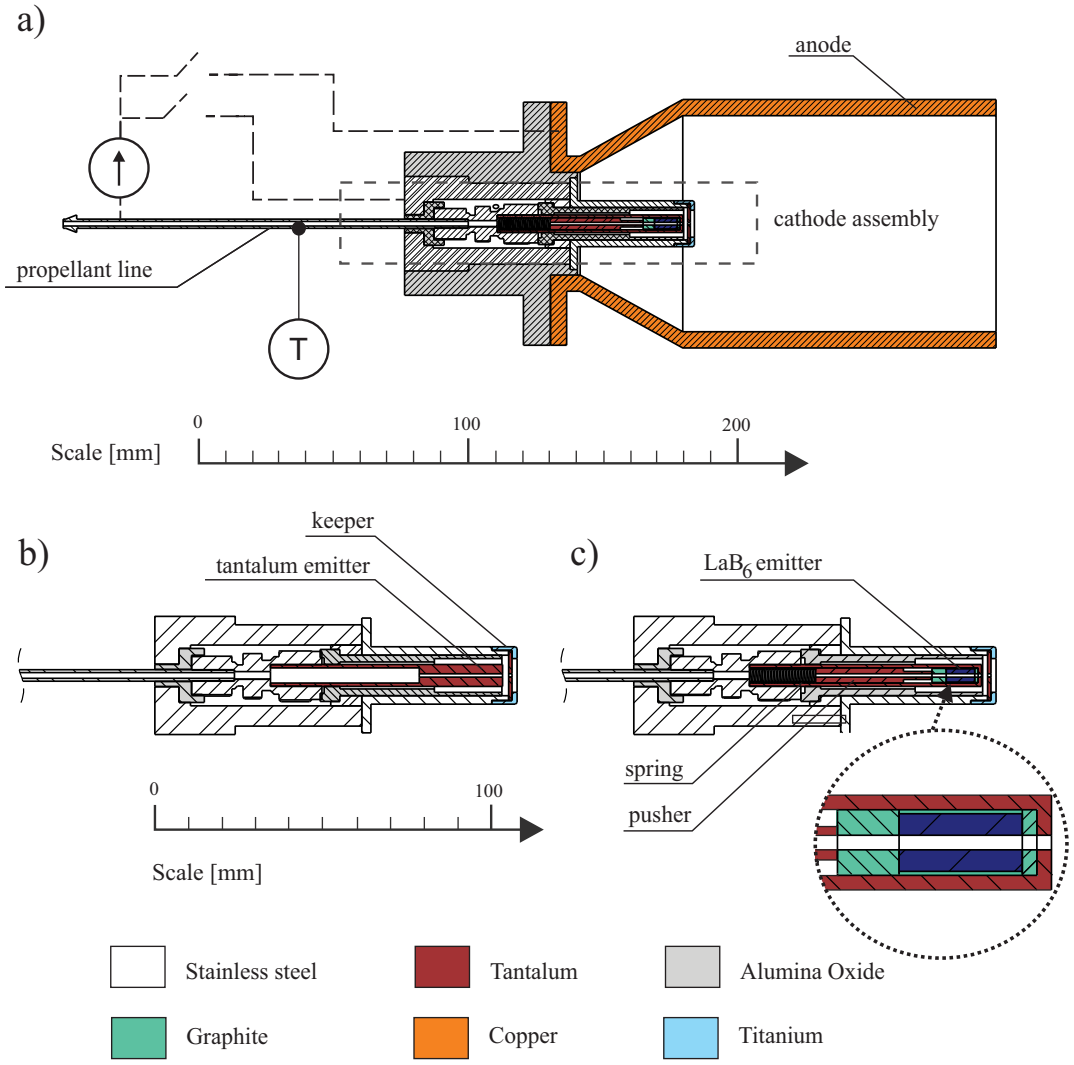

Figure 1: (a) Schematics of tested cathode assemblies. b) with a tantalum emitter, c) with a lanthanum hexaboride emitter. The schematics include the electrical circuit used for the discharge and placement of the temperature sensor (marked T)

from 0.7 - 5.7 Ω the current limit was varied at the MOSFET sub-circuit from 0.35 – 1.85 A. It is important to operate the power supply with a set current below this limit, such that the MOSFET provides transient current limiting, but is not dissipating excessive power once a steady state plasma is achieved. The MOSFET sub-circuit provides additional stability, especially during the ignition phase. The MOSFET sub-circuit is insufficient in the absence of R_k, as the transistor would be required to dissipate the power.

Additionally, the system suffers is subjected to low-frequency oscillations coming from the plasma-power supply coupling.[1] It has been reported[19] that this kind of instability can lead to significant variations in the current (up to 100%) at frequencies < 1 kHz. The typical solution is the application of capacitive filters. In this work, it has been observed that the resistive load introduced for arc prevention also mitigates this instability in the steady-state thermionic operation of the cathode.

2.1 Tantalum-emitter cathode

Arc prevention enabled the realisation of stable plasma discharge in the cathode and further investigation into the time evolution of its electrical characteristics. The cathode exhibits different modes which can be clearly distinguished in the current-voltage traces. Typical current-voltage traces are provided in Figure 3. The ignition sequence begins by turning on the propellant flow, to 4 mg/s of Argon. A flow rate below approximately 2 mg/s cannot maintain the plasma during ignition, while a larger flow rate results in a plasma that rapidly “burns out”, resulting in a small, dim

DOI: 10.13009/EUCASS2023-960

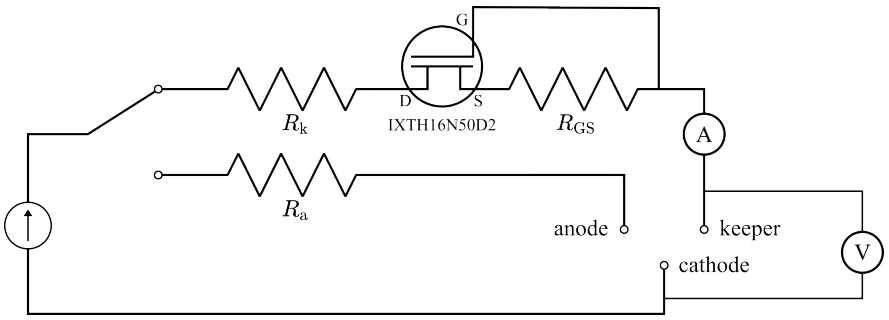

Figure 2: Electronic circuitry implemented to allow reliable ignition of the cathode. For stabilisation and arc prevention, the resistor R_k provides current limiting via Ohm's law, while the depletion mode MOSFET with gate–source resistor, R_{GS}, provides a stricter current limit. Different values of R_{GS} provided control over the current limit during development. The anode circuit is not directly relevant to the cathode ignition but is included for completeness and context.

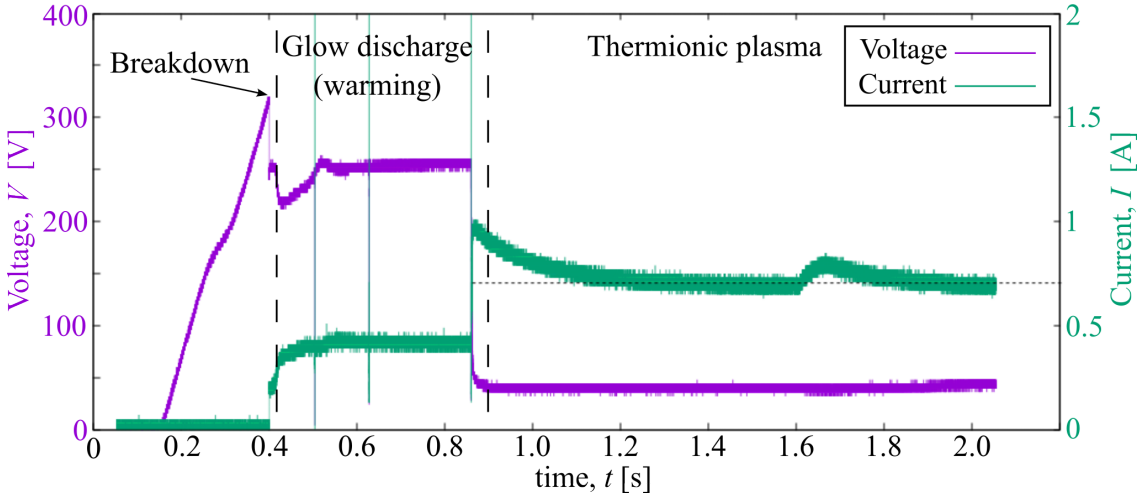

Figure 3: Cathode–keeper voltage (purple) and current (green) plotted over the duration of a typical successful ignition of the tantalum-emitter cathode. The dashed horizontal line indicates the current limit set on the power supply unit.

thermionic plume. To ignite the cathode, the output voltage of the power supply is ramped to 400 V over one second until a Paschen breakdown occurs. The breakdown voltage is dependent on the propellant used, the propellant flow rate, and cathode–keeper geometries that affect the pressure, but is typically on the order of 250 - 300 V. It is found that $R_k \approx 120\ \Omega$ is sufficient to stabilise the ignition.

It takes anywhere from 100 ms to tens of seconds for the plasma to heat the emitter to thermionic temperatures. The time-to-ignition is highly dependent on whether the cathode was already warm from a previous ignition and the current limit. A larger current through the glow plasma heats the emitter faster. The glow discharge is characterised by a small, dim, purple plume, maintained by a cathode–keeper voltage of approximately 200 – 300 V depending on parameters such as the propellant flow rate and keeper geometry. As the plasma transitions to a thermionic mode, the plume becomes larger, bright orange or even white, and there is a significant drop in the keeper voltage while the current rises, as can be seen in Figure 3. Once thermionic, the power supply is operating in a constant-current mode. When ignited, the propellant flow rate and current limit can be adjusted, away from those used for the ignition process. A propellant flow rate of greater than 0.3 mg/s can maintain a thermionic plasma. In fact, if the propellant flow rate is left "high", the thermionic plasma will fade to a relatively small, dim plume. The steady-state keeper voltage is a useful proxy for the output power of the cathode and is highly dependent on parameters such as the propellant flow rate, the set current limit, and the cathode–keeper geometry. Figure 4 shows the keeper voltage at a range of currents and propellant flow rates, for a keeper with a 1 mm orifice. There is a distinctly non-ohmic relationship between current and voltage: lower currents provide less thermal energy to the emitter, so require higher voltages to maintain a plasma. In the operating regime considered, lower propellant flow rates require larger voltages, although by 3 mg/s this appears to have stabilised. Further, both the current and propellant flow rate have an effect on the stability of the resulting plasma. This is indicated in Figure 4 by the fact that only the lowest flow rate of 0.5 mg/s is able to maintain a stable plasma at

DOI: 10.13009/EUCASS2023-960

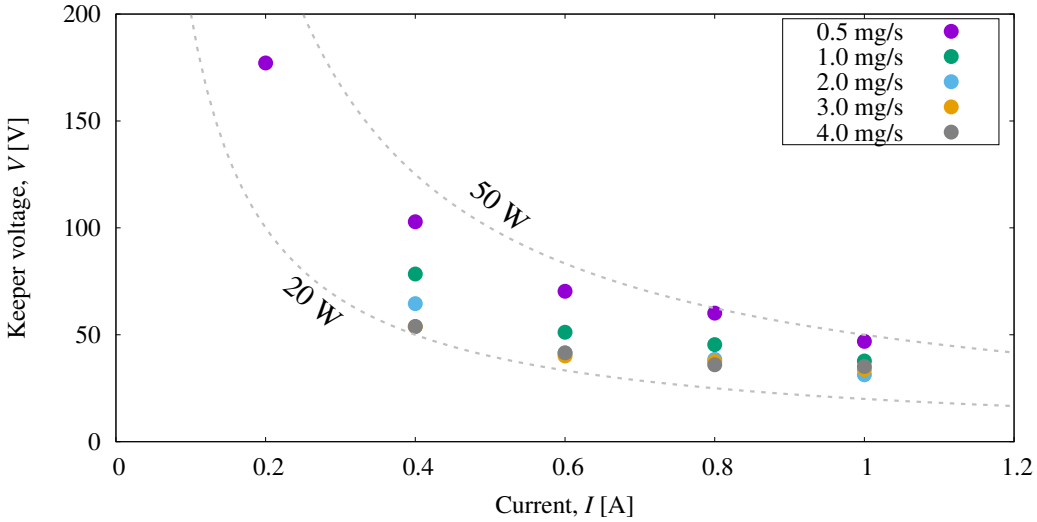

Figure 4: Comparison of the steady-state keeper voltage at a range of currents and argon flow rates, for the tantalum-emitter cathode. The current through the plasma and the keeper voltage is measured once a steady state thermionic emission is reached. Data was obtained by taking the mean of the time-averaged steady-state voltage over three runs at each data point. Using a new tantalum-emitter cathode with a 1 mm keeper orifice.

(a) (b)

Figure 5: Comparisons exhibiting degradation to the tantalum-emitter cathode over time. (a) picture of the cathode tip at installation. After two months of operation a significant amount of mass has been lost in the region marked in dashed yellow lines. (b) picture of the plasma produced by the cathode under identical operating conditions (1.8 A keeper current, 0.5 mg/s argon flow, 1.3 mm keeper orifice) approximately two months apart, with the picture on the left side being saturated due to light emission from the cathode. Pictures are taken looking directly towards the tip of the cathode. Note that in both cases the anode is in place, but is not energized.

0.2 A. Over the course of approximately 150 ignitions during two months of operation, the tantalum-emitter cathode underwent visible degradation, as evidenced in Figure 5a. We observe evidence of melting between the layers of the emitter, and significant loss of mass, due to high-energy ion bombardment. This was most evident at the centre of the emitter, which had receded over 2 mm. In conjunction with visible damage to the cathode, performance characteristics noticeably changed. It was found that larger propellant flow rates were required during the ignition phase – up to 8 mg/s – and the steady-state keeper voltages tended to decrease slightly. Most noticeably, the brightness and size of the plasma plume decreased significantly under identical operating conditions, as exemplified in Figure 5b. It was found that the decreased plasma volume could be at least partially compensated by increasing the current, reducing the propellant flow rate, and increasing the diameter of the keeper orifice. Increasing the keeper orifice was the most effective, but it is worth noting that this in turn alters the parameters required for ignition. For example, an increased propellant flow rate is required to continue operating near the Paschen minimum. Ultimately it is undesirable for the

DOI: 10.13009/EUCASS2023-960

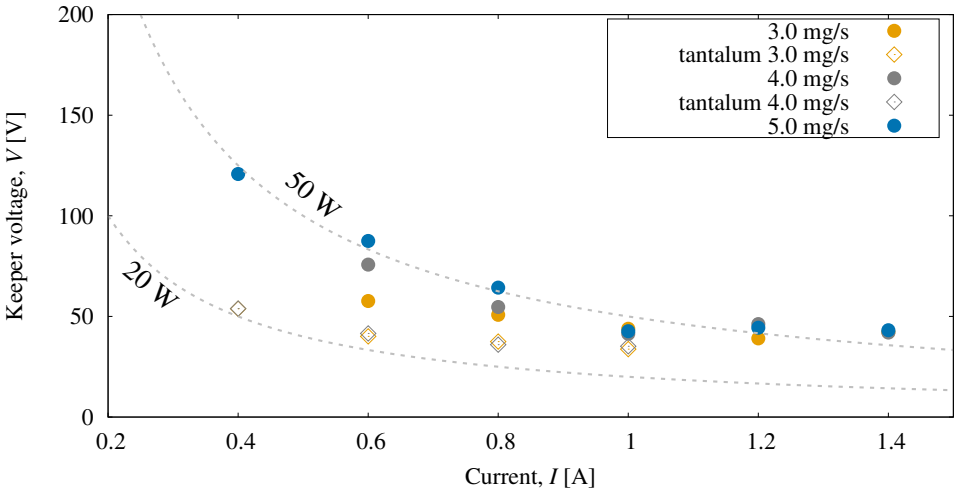

Figure 6: Comparison of the steady-state cathode–keeper voltage at a range of currents and argon flow rates, for the lanthanum hexaboride-emitter cathode with a 1mm keeper orifice. Data from the tantalum-emitter cathode is included as a comparison point for the operating regimes which overlap.

operating characteristics to change so noticeably over a relatively short time frame, especially in the context of an EP thruster designed with space applications in mind.

2.2 Lanthanum hexaboride-emitter cathode

Issues related to tantalum open-ended cathode, manifested in front face erosion can be mitigated by retracting the emitter into the protection of the tantalum tube. The immediate drawback is the reduction in emitter temperature and in turn the thermionic emission. The effect can be reduced with the application of low-work function materials such as LaB_6. The design presented in 1c shows the placement of the emitter within the tantalum tube. The LaB_6 was placed between two graphite washers, and surrounded by a graphite sheath. The inert graphite keeps the LaB_6 isolated from the tantalum, to prevent contamination via diffusion of tantalum during operation. The assembly is kept in place by use of a tantalum pusher and a spring providing a degree of operational flexibility giving the ability to disassemble the cathode if needed. Results presented in Fig.6 show the cathode's current-voltage characteristics. It was found that the cathode was particularly unstable below 3 mg/s of argon flow, or when operated below 1A. The cathode operates in a spot model, although even in the high-current (>1.4A) there is a higher level of instability compared to the tantalum-emitter cathode and the cathode operation moves into a plume mode. Operation in this mode is highly undesirable, as it has been associated with the development of Ion Acoustic Turbulence which in turn led to excessive cathode erosion.[20]

The ignition process is the same as that described for the tantalum-emitter cathode, although it was warmed up with a 1.5A current limit, and the higher level of instability is resolved by increasing the resistive load to $R_k = 400\ \Omega$, and initially ramping the voltage over 60 seconds when inducing plasma breakdown.

Like with the tantalum-emitter cathode, the LaB_6 cathode shows a non-Ohmic relationship in which a smaller current requires a larger voltage. Due to the preferred operation of the LaB_6 emitter in the high-power, high-current, high-mass flow rate regime, the data presented in Figure 6 does not directly match the operating regimes presented for the tantalum-emitter cathode in Figure 4. For the comparable data, the cathode–keeper voltage of the LaB_6-emitter cathode is strictly larger than the tantalum-emitter cathode, indicative of its higher-power operating regime. Further, similarly to the tantalum-emitter cathode, lower currents are achievable if cathode operates with a propellant flow rate corresponding to a higher keeper voltage.

The cathodes show similar modes of degradation with the tantalum tube inlet hole being mainly subjected to erosion. However, after several hours of operation, the degradation was minimal compared to the open-ended tantalum insert. For the LaB_6 cathode the most prominent mode of cathode erosion is the keeper orifice surface.

3. Thermal characterisation

Different discharge characteristics play a crucial role in the energy transfer to the cathode from the power supply, governing the intensity of electron emission to plasma. The evaluation of the role of heat dissipation is therefore

DOI: 10.13009/EUCASS2023-960

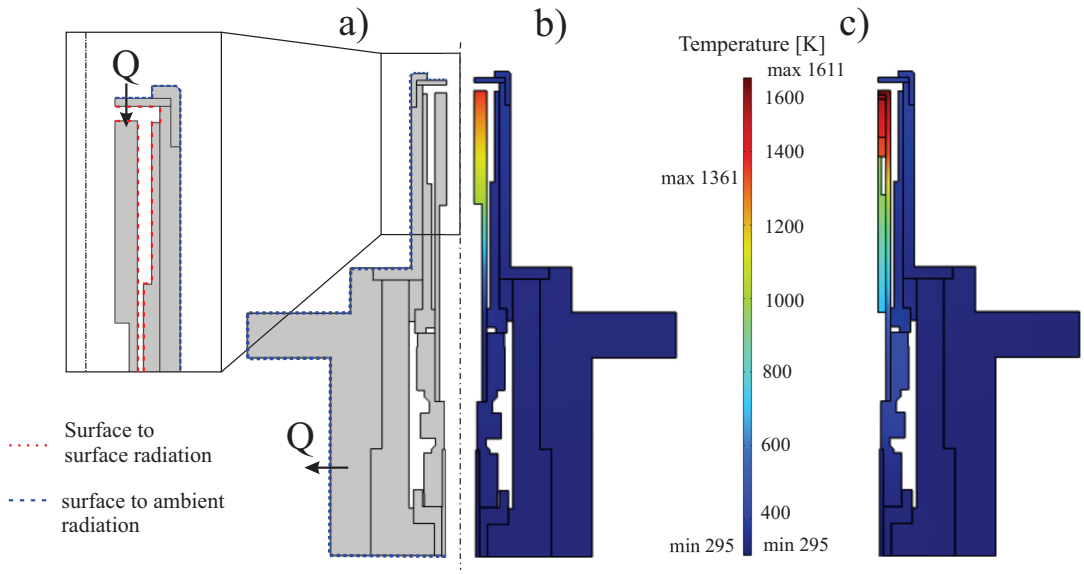

Figure 7: Thermal characterisation of hollow cathodes with a) boundary conditions used for the analysis, b) temperature distribution on tantalum cathode c) temperature distribution on lanthanum hexaboride cathode

of primary concern for cathode designers. Therefore, thermal analysis becomes a useful preliminary analysis tool which guides further development of the design. Assuming the thermal model to be a physical system dominated by conduction and radiation, with heat evaluated based on discharge power allows a level of simplification to be introduced and its validity must be carefully evaluated. In particular, such an approach neglects important relations between self-heating mechanisms coming from ion bombardment, and heat removed through plasma. These aspects were evaluated in the literature and proved to play a role in the overall temperature on the surface of the emitter.[21] Nevertheless, the applicability of the approach through the utilisation of widely available numerical tools accelerates the design process by providing a first-order modelling tool. Due to the complexity related to numerous design parameters, such analysis can be useful, but the conclusion drawn and subsequent application thereof must be cautiously evaluated.

The approach presented in this section is based on the evaluation of a thermal distribution obtained from the energy balance within the partially closed system. The main mechanisms of energy transfer are conduction and radiation. The heat flux transferred due to the surface-to-surface radiation $q = (1 - \rho_s)G - J$, where G is the incoming radiative heat flux, is approached through the calculation of surface radiosity J assuming the grey-body radiation model. The energy input is assumed to be a fully dissipated electric power to the cathode insert and is known from the measurement of current and voltage. The heat is transferred through the insert's front face as shown in Fig. 7a. The thermal cycle for both cathodes follows the same discharge pattern realised at a constant argon flow of 4 mg/s. The energy sink is through the conduction to the outer stainless steel mount, which is clamped around the outer insulator and through the surface to ambient radiation $q = \varepsilon\sigma(T_a^4 - T^4)$, where ε is a surface emissivity, σ Stefan Boltzmann's constant and $T_a = 295$ K measured ambient temperature on chamber walls. The solution was obtained, using the Finite Element Method solving a governing heat equation

$$\rho c_p \frac{\partial T}{\partial t} + \nabla \cdot (\lambda \nabla T) = Q \tag{2}$$

where the material properties of thermal conductivity λ, heat capacity c_p and density ρ. Figure 7a shows boundary conditions used in the model. The temperature is evaluated at the tip of the emitter which is defined as the point closest to the keeper orifice and to the inner channel. The maximum temperature reached by the tantalum and LaB_6 cathodes are shown on 7b and 7c respectively.

As most of the materials in the cathode are subjected to high (>1000 K) temperatures, it is necessary to include temperature dependency in modelling the behaviour of thermal coefficients For tantalum which is used in abundance in both designs, the $\epsilon(T)$ was assumed to vary linearly between 0.136 at 1000 K to 0.232 at 2000 K,[22] heat capacity follows the semi-analytical relation: $c_p(T) = (20.69482 + 17.29992 \cdot (T/1000) - 15.68987) \cdot (T/1000)^2 + 5.608694 \cdot (T/1000)^3 + 0.061581/T^2)$[23] [J/(mol · K)] and $\lambda(T) = 57.5 + 0.0025T$ [W/(m · K)].[24]

The results presented in Fig. 8 show a temperature in time change at the propellant line. The presented result shows one thermal cycle where an initial 700 s warmup phase is followed by a 2.5 hr cool-down process. The thermal warm-up follows a procedure of initial current ramp up to 1.5 A for the 60 s, followed by 20 s of operation in high

DOI: 10.13009/EUCASS2023-960

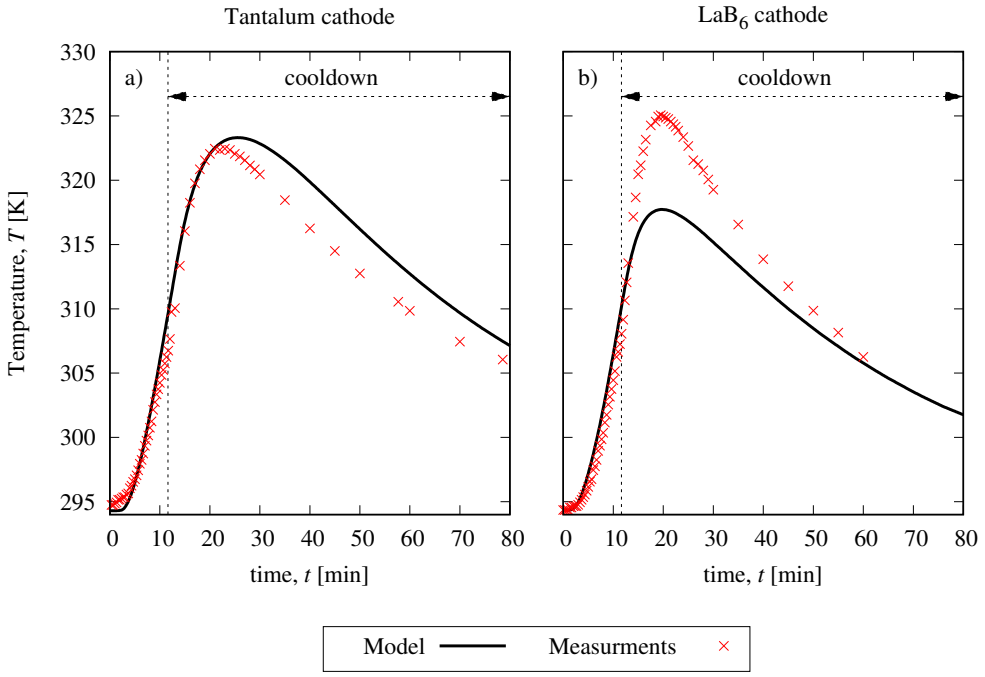

Figure 8: Model validation of a thermal model through the thermal cycling of tantalum (a) and lanthanum hexaboride cathodes (b).

current mode and 20 s ramp down to target 0.8 A. The cycle was run for both tantalum (in Fig. 8a) and LaB_6 cathodes (in Fig. 8b). The presented results show a good agreement between the model and measurements. Modelled temperature increases during the warm-up process and closely match measurement values. LaB_6 cathode reaches a maximum temperature of 328 K, which is 10 K higher than the tantalum cathode, and the resulting difference may be related to higher dissipated power for the same operating current. The observed steeper cool-down rate for the LaB_6 cathode indicates that the cathode can be characterised by a higher thermal thermal inertia. Considering the overall higher mass of the LaB_6 it indicates poor thermal contact with the inner components at the cathode tube. Although, the model predicts well the temperature of the tantalum cathode it under-predicts the temperature of the LaB_6 cathode. Results presented in Fig. 8b although stay in good agreement with the measurement during the warm-up cycle misrepresents the maximum temperature by 10K. This discrepancy can be attributed to the unknown tolerances on the graphite-emitter assembly and related thermal contact. It must be noted, that the temperature measurements implicitly contain considerable uncertainty which is not presented in Fig.8. Although the presented absolute value may vary considerably, the presented true absolute values, and the differential readings should provide sufficiently accurate estimates, to within a few Kelvins.[25]

Results presented in Fig. 9a and 9b show a measured voltage profile. The voltage drop for the tantalum cathode follows a warm-up period. On the contrary, the LaB_6 cathode doesn't have clearly identifiable warmup periods and the thermionic emission follows closely the breakdown. The transition between states closely follows a rapid increase in temperature shown in Fig. 9c and 9d. This provides additional weight to the validity of the proposed model for modelling transient warm-ups. Therefore, the model can provide indicative temperatures for evaluating the parts of the cathode assembly, which are not easily accessible for measurements. The model shows distinguishable differences in the temperature rise of both cathode types. Although the model shows that both reach a similar temperature of around 1400 K it takes more than 400 s longer for the LaB_6 cathode to reach it. This gives some quantitative evidence for the effect of embedding the emitter within the tantalum tube and can be related to the added thermal inertia. The role of the temperature gradient is not observable, due to high power delivered to LaB_6 cathode during the discharge. The total emission electron current is calculated as a current density integrated over the emitter surface $I_e = \int j_e(T)dA$ is presented on 8e and 8f. Quantification of the temperature within the cathode during operation can be done via comparative studies of both cathode emission profiles triggered by the heat conducted to the emitter. In both cases, the transition to the thermionic state occurs at a similar level of electron emission $I_e \approx 10^{-10}$ mA. In overall, the emission from the LaB_6 cathode is orders of magnitude higher than for tantalum with a peak at $T_{LaB_6} = 8$ mA compared to $T_{LaB_6} = 0.8$ μA. The design decision to embed the emitter within the tantalum tube has no negative effect on the

DOI: 10.13009/EUCASS2023-960

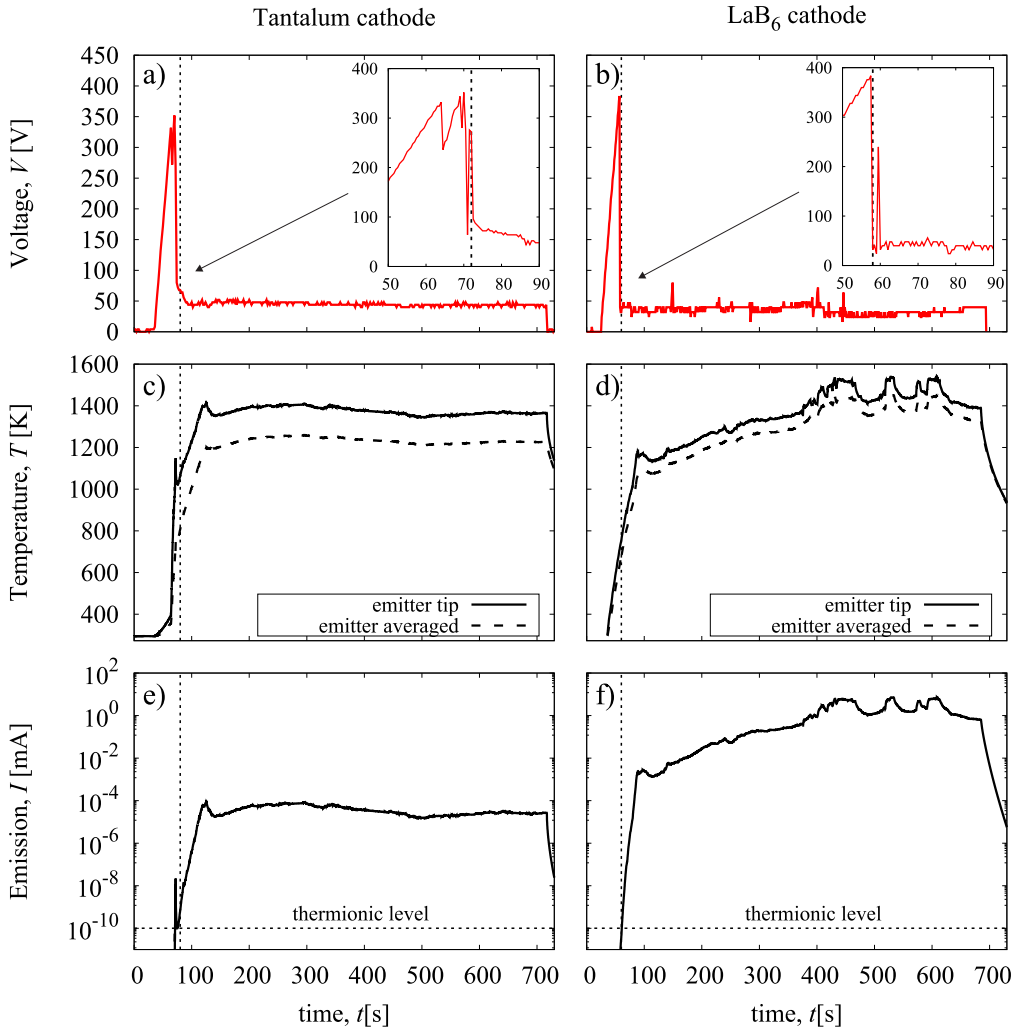

Figure 9: Keeper discharge voltage for tantalum (a) and LaB_6 cathodes, compared to temperature distribution at cathodes' tip (c)(d) and expected electron emission intensity due to heat transfer within the cathodes (e)(f) All numerical results are presented in black and experimental in red.

maximum cathode temperature except for the delay in reaching peak emission. The design based on LaB_6 has a longer lifetime and can be used to minimise discharge power requirements while maintaining high emissivity.

4. Conclusions

The work presents the results obtained during the development and characterisation of two heaterless hollow cathodes: one based on an open-ended tantalum emitter and the second based on embedded lanthanum hexaboride. Both cathodes deliver discharges between 20-50 W, operating in the range of 0.6-1.4 A, and exhibit oscillatory behaviour which was mitigated by the use of a current-limiting circuit and resistive load. The presented results are based on voltage-current characterisation and highlight design trade-offs between these two cathode types.
The tantalum cathode was able to operate more stably and delivers discharges with lower voltage requirements when compared to LaB_6 and operates at lower mass flow rates (down to 0.4 mg/s). However, its operation was also characterised by a high erosion rate which impacted its characteristics after 10 s hours of operation. On the contrary, the LaB_6 cathode although requiring higher discharge power, showed no signs of erosion during a comparable testing period.

A first-order thermal analysis was combined with experimental measurements and was shown to be a reliable tool to estimate the temperature distribution in hard-to-access components, such as the emitter during the initial transient state. The temperature at the tip of both emitters was shown to reach approximately 1400 K which corresponds to 0.8 mA and 8 mA emission for tantalum and LaB_6 cathode respectively. In both cases, similar emission triggers a voltage transition to a thermionic emission state. The associated temperature for tantalum and LaB_6 cathodes is approximately 1000 K and 600 K.

DOI: 10.13009/EUCASS2023-960

5. Acknowledgments

This work was funded by the New Zealand Ministry of Business, Innovation and Employment under contract RTVU1916.

References

[1] D. Lev, I. Mikellides, D. Pedrini, D. Goebel, B. Jorns, and M. Mcdonald. Recent progress in research and development of hollow cathodes for electric propulsion. *Plasma Physics*, 3, 06 2019.

[2] C. Koppel and D. Estublier. The smart-1 hall effect thruster around the moon: In flight experience. In *29th International electric propulsion conference*, page 119. Citeseer, 2005.

[3] A. Kodys, J. Pilchuk, M. Glogowski, J. Trescott, J. Pucci, and B. Koch. Initial flight operations of the geostar-3 electric propulsion system. In *2018 Joint Propulsion Conference*, page 4719, 2018.

[4] L. Chenguang, N. Zhongxi, Z. Ximing, and Y. Daren. Design of magnetically enhanced hollow cathode micro-thruster: Concept and experimental research. *Acta Astronautica*, 207:257–264, 2023.

[5] G. Becatti, R. W. Conversano, and D. M. Goebel. Demonstration of 25,000 ignitions on a proto-flight compact heaterless lanthanum hexaboride hollow cathode. *Acta Astronautica*, 178:181–191, 2021.

[6] M. S McDonald, A. D. Gallimore, and D. M. Goebel. Note: Improved heater design for high-temperature hollow cathodes. *Review of Scientific Instruments*, 88(2):026104, 02 2017.

[7] G. Aston. Hollow cathode startup using a microplasma discharge. *Review of Scientific Instruments*, 52(8):1259–1260, 1981.

[8] D. Pedrini, C. Ducci, U. Cesari, T. Misuri, and M. Andrenucci. Sitael hc1 low-current hollow cathode. *Aerospace*, 7(7), 2020.

[9] J. H. Hsieh, M. Shen, Y. Li, and P. Huang. Development of a lanthanum hexaboride hollow cathode for a magnetic octupole thruster. *Vacuum*, 214:112146, 2023.

[10] N. Gondol and M. Tajmar. Design of a hollow cathode thruster: concepts, parameter study and initial test results. *CEAS Space J*, 14:65–77, 2022.

[11] H. Kasuga, J. Jeong, K. Mizutani, A. Iwakawa, A. Sasoh, K. Kojima, T. Kimura, Y. Kawamata, and M. Yasui. Operation characteristics of applied-field magnetoplasmadynamics thruster using hollow cathode. *Trans. JSASS Aerospace Tech. Japan*, 16(1), 2018.

[12] J. Balkenhohl, J. Glowacki, N. Rattenbury, and J. Cater. A review of low-power applied-field magnetoplasmadynamic thruster research and the development of an improved performance model. *Journal of Electric Propulsion*, 2(1), 2023.

[13] J. Glowacki, R. Badcock, and N. Long. Design analysis of a plasma thruster with superconducting magnets. *AIAA Propulsion and Energy 2019 Forum*, August 2019.

[14] A. S. Voronov, A. A. Troitskiy, I. D. Egorov, S. V. Samoilenkov, and A. P. Vavilov. Magnetoplasmadynamic thruster with an applied field based on the second generation high-temperature superconductors. *Journal of Physics: Conference Series*, 1686:012023, December 2020. Publisher: IOP Publishing.

[15] J. R. Olatunji, H. W. Weijers, N. M. Strickland, and S. C. Wimbush. Modelling the quench behavior of an ni hts applied-field module for a magnetoplasmadynamic thruster undergoing a 1kw discharge. *IEEE Transactions on Applied Superconductivity*, 33(5):1–6, 2023.

[16] D. M. Goebel and R. M. Watkins. Compact lanthanum hexaboride hollow cathode. *Review of Scientific Instruments*, 81(8):083504, 08 2010.

[17] E. K. Storms and B. A. Mueller. A study of surface stoichiometry and thermionic emission using LaB6. *Journal of Applied Physics*, 50(5):3691–3698, 07 2008.

[18] C. J. Smithells. *Metals Reference Book*, volume III. Butterworths, London, 1967.

DOI: 10.13009/EUCASS2023-960

[19] D. M. Goebel, K. Jameson, I. Katz, and I. Mikellides. Potential fluctuations and energetic ion production in hollow cathode discharges. *Physics of Plasmas*, 14(10), August 2007. 103508.

[20] P. Georgin, Benjamin A. Jorns, and Alec D. Gallimore. An experimental and theoretical study of hollow cathode plume mode oscillations. In *35th International Electric Propulsion Conference*, Atlanta, USA, 2017.

[21] U. Kokal, N. Turan, and M. Celik. Thermal analysis and testing of different designs of lab6 hollow cathodes to be used in electric propulsion applications. *Aerospace*, 8(8), 2021.

[22] D.B. Langmuir L. Malter. Resistance, emissivities and the melting point of tantalum. *Phys. Rev. Phys. Rev*, 55(8), 1939.

[23] M.W.Jr. Chase. Nist-janaf themochemical tables. NIST, 1998. Fourth Edition, J. Phys. Chem. Ref. Data, Monograph 9.

[24] I.V. Savchenko and S.V. Stankus. Thermal conductivity and thermal diffusivity of tantalum in the temperature range from 293 to 1800 k. *Thermophysics and Aeromechanics*, 15(4), 2008.

[25] E. Webster. Base-metal thermocouple tolerances and their utility in real-world measurements. *Measurement Science and Technology*, 32(8):085007, may 2021.